Fractal growth of viscous fingers: quantitative characterization of a fluid instability phenomenon

Johann Nittmann*, Gérard Daccord* & H. Eugene Stanley†

* Etudes et Fabrication Dowell Schlumberger 42003 St Etienne, France
† Center for Polymer Studies and Department of Physics, Boston University, Boston, Massachusetts 02215, USA

What happens when one attempts to push water through a fluid of higher viscosity? Under appropriate experimental conditions, the water breaks through in the form of highly branched patterns called viscous fingers. Water was used to push a more viscous but miscible, non-newtonian fluid in a Hele-Shaw cell. The resulting viscous finger instability was found to be a fractal growth phenomenon. Reproducible values of the fractal dimension d_f *were found and were interpreted using a modification of the diffusion limited aggregation model.*

WHEN one attempts to use a low viscosity fluid (like water) to push high viscosity fluid (like oil), there arises a fluid instability phenomenon termed the 'viscous fingering instability' in which the low viscosity fluid forms characteristic fingers extending well into the high viscosity fluid[1–4]. In addition to its obvious interest in enhanced oil recovery by water flooding, and other practical applications, this phenomenon is of considerable basic interest and is not understood at present. It may be studied in detail in the laboratory using a Hele-Shaw cell, which is a pair of transparent plates separated by typically 0.5 mm. The space between the plates is filled with high viscosity fluid and the low viscosity fluid is injected. Normally, the interfacial tension between the two fluids is high and the low viscosity fluid forms non-fractal patterns that resemble the fingers of a glove[1,2]. Fractal phenomena are found to be associated with a range of random systems[5–8]. For this reason it is of interest to inquire whether or not there exist experimental conditions under which viscous fingers obey a fractal symmetry.

Experiments

Fractal structures in nature typically occur when randomizing effects dominate over stabilizing effects. Hence to find a fractal structure we must eliminate stabilizing effects so that the randomness can dominate a structure. To this end we shall minimize the role of interfacial tension[1,2] as well as intermolecular diffusion[3]. Therefore, we chose a viscous fluid with zero interfacial tension against water, an aqueous polymer solution of high relative molecular mass polysaccharide for which the mixing time is very slow compared with the time of the experiment.

Since the viscosity difference is the driving force for the instability, a high viscosity is desirable. Hence we use a non-newtonian fluid: the low-shear regions have high viscosity while the shear thinning character of the fluid makes it easy to pump it through the narrow gap of the Hele-Shaw cell without causing

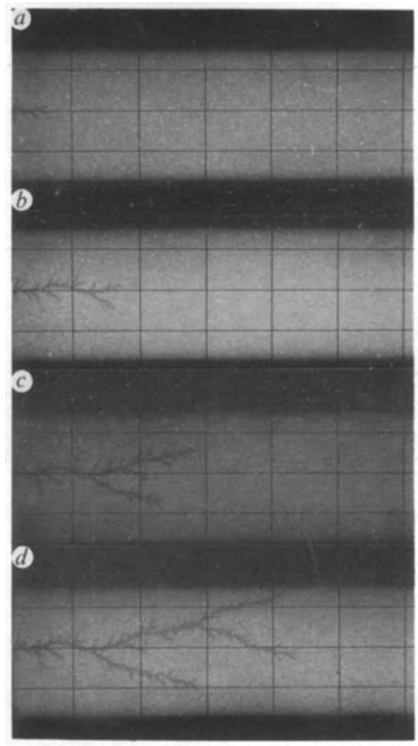

Fig. 1 Typical viscous finger created by water advancing into a Hele-Shaw cell filled with a non-newtonian fluid with zero interfacial tension (experimental conditions described in the text). The time interval between successive photographs is typically 5 s. The grid rectangles have dimensions 3 cm × 5 cm. The water, dyed with methylene blue, is injected under force from a single inlet on the left wall into an aqueous polymer solution whose viscosity varies between 10^3 and 10^4 cP depending on the water velocity.

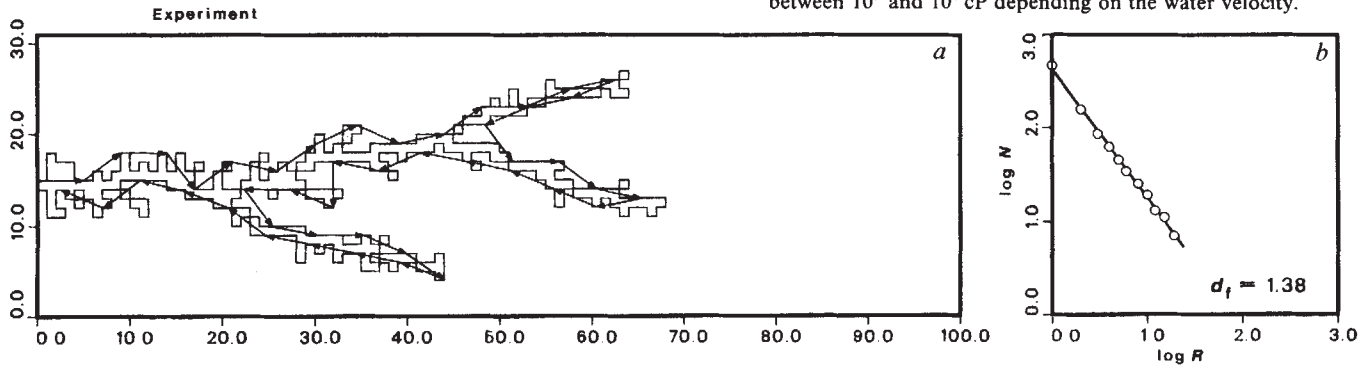

Fig. 2 Schematic illustration of the determination of d_f from experimental data of Fig. 1. *a*, Illustration of how the contour length of the digitized finger is measured with a ruler of length $R = 5$. *b*, The slope of the straight line gives $-d_f$, from which we find $d_f = 1.39$.

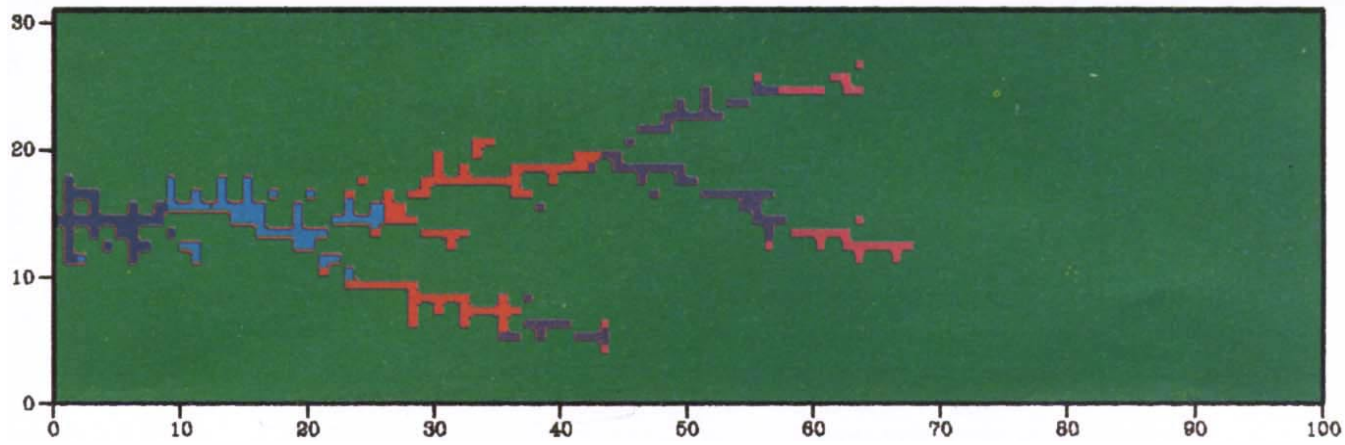

Fig. 3 Digitized representation of the viscous finger of Fig. 1. The colour coding is an indication of the time evolution of the instability, the order being dark blue, light blue, red, violet and pink. The colour coding is for comparison with the model calculations of Fig. 4.

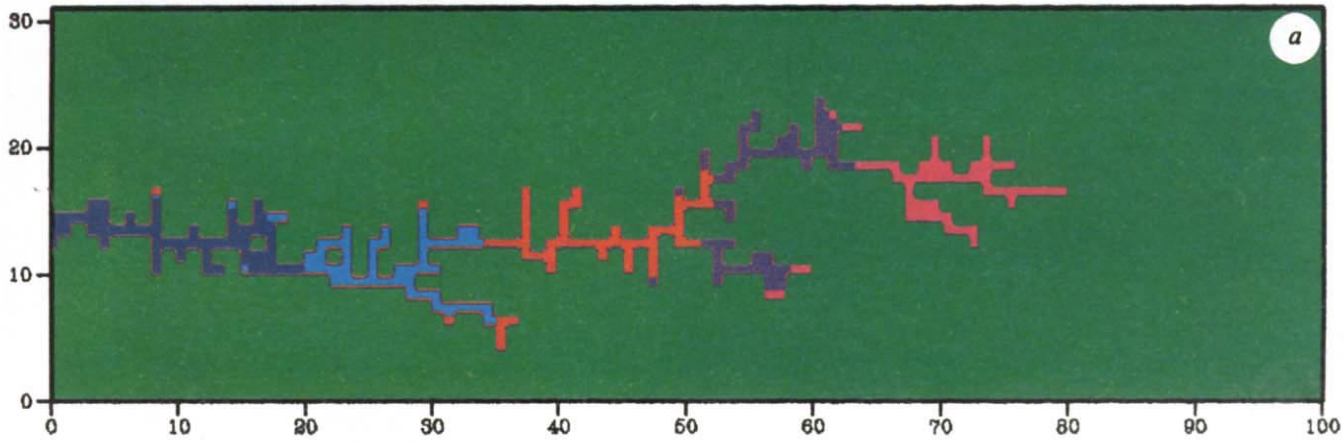

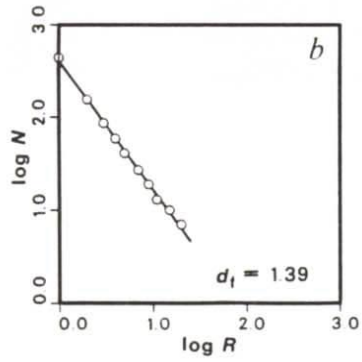

Fig. 4 Results of model calculation for the ratio $W_{HS}/W_f = 30$, corresponding to the experiments of Fig. 1. *a*, Colour coding indicates the time of arrival of the random walker, the order being dark blue, light blue, red, violet and pink; each colour represents 20% of total time. Comparison with Fig. 3 confirms the agreement between experiment and the model. *b*, The fractal dimension of the aggregate shown is 1.39, in agreement with the analysis of the experimental data of Fig. 2.

bending of the plates. In contrast, tests with newtonian fluids were limited to a viscosity of 100× that of water, and steady fine-structured fingering patterns were not observed.

We placed the polymer solution into a perpex Hele-Shaw cell[8] of thickness 0.5 mm, length 0.9 m and width 0.1 m. Water dyed with methylene blue was injected at one end at a variety of flow rates between 0.4 and 40 ml min^{-1}. We used three different polysaccharides and have varied the polymer concentration from 0.24 to 1.2 wt %. The viscosity of the polymer solution varies between 10^3 and 10^4 cP depending on the water velocity. We have also repeated measurements using a Hele-Shaw cell of thickness 1.0 mm. The resulting viscous finger patterns were random and highly branched (Fig. 1, *a*–*d*).

Analysis

Visual examination of these patterns reveals the striking presence of structure at many different length scales. Hence it seemed appropriate to attempt to analyse the structure of a viscous finger using the concept of self-similarity or fractals[5]. To this end, we first digitized the fingering patterns (Fig. 3) using a pixel size equal to the characteristic thickness of a viscous finger. We then analysed the patterns as follows. We measured the total exterior perimeter length using a 'ruler' of length $R = 1$, measured in units of a pixel. Then we repeated the same operation for a range of increasing R values up to $R = 20$ (Fig. 2*a*). The apparent length of any fractal, in units of R, decreases as R^{-d_f} (Fig. 2*b*)[5,9]. The d_f of the external perimeter is the same as the d_f of the total mass if loops do not occur on all length scales[5]. We find the quantitative parameter, $d_f = 1.40 \pm 0.04$, which characterizes viscous fingers for a wide range of polysaccharides, polymer concentrations and water flow rates, suggesting that viscous fingers indeed have a reproducible and universal fractal dimension.

As a second method, we placed an imaginary box of edge L on each point of the finger. For each box, we counted the number of points (the total mass) inside the box. As L increases, this mass should scale as L^{d_f} if the finger has a fractal structure[10]. We find that Method 2 gives smaller values for d_f than predicted by Method 1. The difference is ~8 % and is explained by the fact that a large proportion of the finger points lie on the

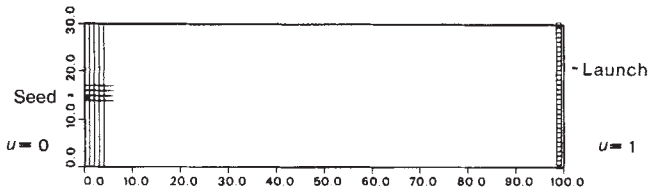

Fig. 5 The basic geometry of the generalized Witten–Sander model used to simulate viscous fingers. Random walkers are released from a randomly chosen point on the right wall, and 'die' if they strike the lateral or end walls.

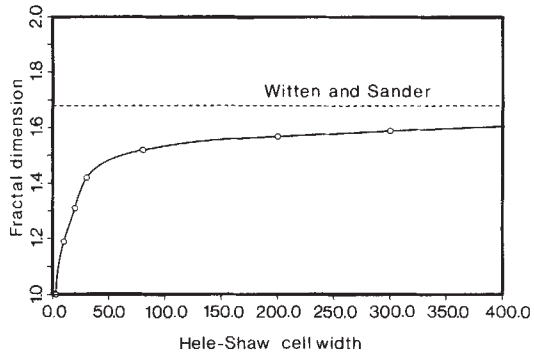

Fig. 6 Dependence on W_{HS} of the apparent value of the fractal dimension, d_f.

perimeter of a particular pattern and boxes centred at these points will cover much unoccupied area outside the structure. For the large-scale numerical simulations discussed below, the number of points on the perimeter is small compared with the total number of points; both methods give identical fractal dimensions.

Statistical model

The mean velocity, v, of a viscous fluid in a Hele-Shaw cell is given by the gradient of a potential $\phi = -(b^2/12\,\mu)\,P$, where b is the plate separation, μ is the shear viscosity and P is the fluid pressure[11]. For incompressible fluids, div $v = 0$; hence we obtain a Laplace equation for the potential distribution

$$\nabla^2\phi = 0 \qquad (1)$$

If, as in our case, the viscosity ratio between the two fluids is very large, we can approximate the potential in the less viscous fluid to be a constant ($\phi = \phi_0$). At the outlet, ϕ takes on a different value $\phi = \phi_1$.

With these boundary conditions, equation (1) is identical to the Laplace equation describing the probability $u(r, t)$ of a random walker to be at the point r at the time t[12,13]. This is similar to diffusion-limited aggregation (DLA)[13–16], so we propose the following quantitative model for viscous fingering. Place a seed particle at the origin (Fig. 5) and release a random walker from a randomly chosen point on the opposite wall. If the random walker hits the seed, it sticks, whereas if it hits any of the four walls, it 'dies' and a new walker is released. For the simulation, we have chosen our 'Hele-Shaw' cell width $W_{HS} = 30$ (in units of a lattice constant), as the experimental value of $x = W_{HS}/W_f$ is ~30, with W_f the characteristic size of a single finger. Formally, the probability $u(r, t)$ can be mapped onto the fluid potential $\phi(r, t)$ described above, $u(r, t) = (\phi - \phi_0)/(\phi_1 - \phi_0)$. Thus, $\phi - \phi_0$ in the finger corresponds to $u = 0$ in the aggregate, whereas $\phi = \phi_1$ at the outlet maps to $u = 1$ at the source of random walkers.

Two striking features of the actual viscous finger experiments are mirrored by our statistical model. The first of these is the tendency of a growing side branch to die out after a relatively short period of growth. The second is the fact that the entire viscous finger strongly avoids coming even moderately close to the lateral walls of the Hele-Shaw cell. Both effects are seen clearly in the model and arise from a common source, 'screening'[13–16]. This screening can be understood as follows. A random walk, statistically speaking, sticks to the tips of the growing aggregate so that the main trunk of the aggregate effectively shields the smaller side fingers. As the lateral walls absorb the random walkers, they act as 'ghost fingers': the viscous finger and the wall together form an essentially impenetrable deep fjord. This can be seen dramatically by the colour coding of Fig. 4, where the last random walkers to arrive, coloured pink, rarely reach the side fingers and never penetrate the deep fjord between the aggregate and the wall.

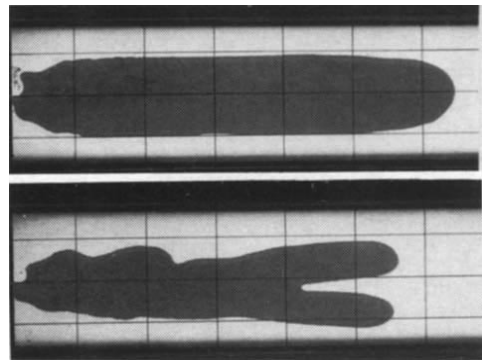

Fig. 7 A viscous finger created by water advancing into a Hele-Shaw cell filled with a newtonian fluid, oil. Two different capillarity numbers are used: *a*, $N_{ca} = 0.08$; *b*, $N_{ca} = 0.16$.

Calculating d_f as described above, we find $d_f = 1.41 \pm 0.05$ (see Fig. 5), a value remarkably close to the experimental value but considerably different from the value $d_f = 1.68 \pm 0.04$ for DLA[17]. Could this difference arise from the geometric constraint of the lateral walls? To test this possibility, we made additional simulations for a range of values of x. We find (Fig. 6) that the apparent value of d_f increases smoothly from $d_f \cong 1$ (for $x \cong 1$) to $d_f \cong 1.60$ (for $x \cong 10^3$). To check this prediction, we also performed experiments for a Hele-Shaw cell half as wide ($x = 15$) and find that $d_f = 1.12 \pm 0.04$, consistent with the predicted value of Fig. 6. What is the source of this apparent dependence of d_f on W_{HS}? At first sight, one might be tempted by an analogy with a growing polymer chain in the same confining geometry; it takes on the bulk value of d_f until it has grown sufficiently to sense the presence of the lateral walls. However, our problem is quite different, since the lateral walls strongly influence even the initial stages of finger growth because the incoming random walks are strongly influenced by the absorbing lateral and end walls. Hence the small fingers cannot capture enough mass to achieve the full DLA structure (this fact becomes especially clear if we consider very small values of W_{HS}). So while for the polymer problem d_f crosses over directly from its bulk value to its ultimate value of $d_f = 1.0$, for the Hele-Shaw fingering problem d_f never takes on its bulk value but instead takes on a smaller value that depends monotonically on W_{HS} (Fig. 6), crossing over ultimately to $d_f = 1$ when $R \gg W_{HS}$.

Discussion

We consider here the relation of the present experiments to previous work on viscous fingering. The classic Saffman–Taylor work did not produce ramified fractal structures. To obtain fine-structured instability patterns for an immiscible fluid system, the critical wavelength λ_c of a perturbation[2,18], defined as $\lambda_c = k[b^2/(12\,N_{ca})]^{1/2}$ has to be much smaller than W_{HS}. N_{ca} is the capillarity number, defined as $N_{ca} = \mu v/\sigma$ (σ is the interfacial tension) and corresponding to the ratio of viscous forces to capillarity forces: k is a dimensionless parameter that depends on the contact angle between the two fluids and the plates (wettability)[18]. We have also performed Saffman–Taylor type experiments with an immiscible newtonian oil-water system with varying flow velocity v, and Fig. 7 indicates that a change

in the flow condition from $N_{ca} = 0.08$ to 0.16 introduces a bifurcation into fingers when the finger thickness exceeds twice λ_c[19]. A continuation of this process would presumably create smaller and smaller fingers with a tree-like structure, but would require a further increase in the capillarity number or a decrease of the plate distance b. We cannot test the possibility that newtonian fluids with very low interfacial tension and negligible intermolecular diffusion but with a very high viscosity ratio, might give rise to similar fractal instability patterns, as our experiments were limited by the finite strength of the cell. By using water and a non-newtonian water-based fluid, we obtained a flow with an infinite capillarity number and a high viscosity ratio in regions where shear stresses are low. We believe both aspects are important and explain the difference from the Saffman–Taylor results.

Our present findings can be applied to the basic physics underlying petroleum science[4,20]. In the traditional '5-spot well configuration', four production wells are drilled at the corners of a large square and CO_2 (or a low viscosity fluid with a very low interfacial tension with oil) is then pumped into a fifth injection well in the centre. The CO_2 plays the role of the water in our model experiments, whereas the oil is analogous to the polymer solution. Large-scale viscous fingering phenomena not bounded by the walls of a Hele-Shaw cell occur and drastically reduce the efficiency of the oil recovery. The observed viscous fingers are quasi-two-dimensional as the thickness of the rock formation is typically several orders of magnitude less than the separation of the injection and production wells. It is therefore customary to assume that the patterns observed in the quasi-two-dimensional Hele-Shaw cells are relevant to the observed macroscopic phenomena. The similarity in the mathematical description of flow through porous media and the Hele-Shaw cell have been observed previously[1]. Thus, our experiments and model calculations strongly suggest that the viscous fingers observed in a 5-spot pattern are rich geometrical structures possessing a scale-invariant symmetry and quantitatively characterized by a fractal dimensionality.

Conclusion

There is no complete theory of miscible viscous fingering, perhaps because there was no quantitative parameter to characterize viscous fingers. Here, we find that viscous fingers are fractals and that their many different random structures have the identical value of the fractal dimensionality. This suggests that the physical basis of the viscous fingering instability is analogous to that of other second-order phase transitions that obey the same sort of scale invariant symmetry found here for viscous fingers[21]. Recent work supports our point of view: quasi-two-dimensional dielectric breakdown seems to exhibit the same sort of fractal structure that we find for the viscous fingering instability[22]. That these two breakdown phenomena should be related is plausible in light of the parallels in the equations describing them[23].

We thank R. Lemanczyk, P. Rossi and the management of Dowell Schlumberger for their encouragement during this work. The Center for Polymer Studies is supported by grants from NSF and ONR. We also thank F. Leyvraz, P. Meakin and J. D. Sherwood for helpful discussions.

Note added in proof: Since acceptance of this article, we have learned of independent work on viscous fingering, both from the experimental (ref. 24, and L. M. Sander and E. Ben-Jacob, personal communication) and theoretical[25,26] points of view.

Received 31 October 1984; accepted 24 January 1985.

1. Saffman, P. G. & Taylor, G. I. *Proc. R. Soc.* **A245**, 312-329 (1958).
2. Chuoke, R. L., Van Meurs, P. & Van der Poel, C. *J. petrol. Tech.* **11**, 64-70 (1959).
3. Stalkup, F. I. *Miscible Displacements* (Soc. of Petroleum Eng., AIME, N.Y., 1983).
4. Hele Shaw, J. S. S. *Nature* **58**, 34-36 (1898).
5. Mandelbrot, B. B. *The Fractal Geometry of Nature* (Freeman, San Francisco, 1982).
6. Brady, R. M. & Ball, R. C. *Nature* **309**, 225-229 (1984).
7. Avnir, D., Farin, D. & Pfeiffer, P. *Nature* **308**, 261-263 (1984).
8. Matsushita, M., Sano, M., Hayakawa, Y., Honjo, H. & Sawada, Y. *Phys. Rev. Lett.* **53**, 286-289 (1984).
9. Powles, J. G. & Quirke, N. *Phys. Rev. Lett.* **52**, 1571-1574 (1984).
10. Forrest, S. L. & Witten, T. A. *J. Phys.* **A12**, L109-112 (1979).
11. Lamb, H. *Hydrodynamics* (Cambridge University Press, London, 1932).
12. Chandrasekhar, S. *Rev. mod. Phys.* **15**, 1-89 (1943).
13. Witten, T. A. & Sander, L. M. *Phys. Rev. Lett.* **47**, 1499-1501 (1981).
14. Witten, T. A. & Sander, L. M. *Phys. Rev.* **B27**, 5685-5697 (1983).
15. Herrmann, H. J. *Phys. Rep.* (in the press).
16. Stanley, H. E. *Fractals in Statistical Physics* (Oxford University Press, New York, 1985).
17. Meakin, P. *Phys. Rev.* **A27**, 1495-1507 (1983).
18. Peters, E. J. & Flock, D. L. *J. Soc. petrol. Engng* **21**, 249-258 (1981).
19. Paterson, L. *J. Fluid Mech.* **113**, 513-529 (1981).
20. Todd, M. R. & Longstaff, W. J. *J. petrol. Tech.* **253**, 874-882 (1972).
21. Stanley, H. E. *Introduction to Phase Transitions and Critical Phenomena* (Oxford University Press, 1971).
22. Niemeyer, L., Pietronero, L. & Wiesmann, H. J. *Phys. Rev. Lett.* **52**, 1033-1036 (1984).
23. Paterson, L. *Phys. Rev. Lett.* **52**, 1621-1624 (1984).
24. Maher, J. V. *Phys. Rev. Lett.* (submitted).
25. Tang, C. *Phys. Rev. A* (submitted).
26. Kadanoff, L. P. *J. stat. Phys.* (submitted).

LETTERS TO NATURE

A very bright water vapour maser source in the galaxy NGC3079

Aubrey D. Haschick* & Willem A. Baan†

* Haystack Observatory, Massachusetts Institute of Technology, Westford, Massachusetts 01886, USA
† Arecibo Observatory, Arecibo, Puerto Rico 00612

The 6_{16}–5_{23} transition of water vapour at 22.235080 GHz has been found in our Galaxy to be associated with regions of young star formation[1,2]. H_2O maser emission was detected initially in an external galaxy by Churchwell *et al.*[3]. To extend the range of detected properties of 'star burst' galaxies (galaxies showing an enhanced star formation from their optical spectra) we undertook an initial survey for H_2O maser emission in this type of galaxy, but with negative results. Here we report on the subsequent extension of this survey to spiral galaxies displaying continuum radio emission, which is also an indication of star formation activity. We have detected the most luminous H_2O maser source yet reported, ~500 $L_\odot$, in the galaxy NGC3079. OH absorption was also detected in this galaxy and we suggest that maser amplification of the nuclear radio source causes the observable H_2O emission.

The 30 galaxies for the survey reported here were selected from lists[4,5] of bright spiral galaxies containing radio sources having both compact and extended components. The observations were carried out in March, April and May 1984 using the 37-m radio telescope of Haystack Observatory, equipped with a maser receiver and a 1,024 channel digital auto-correlator. The system temperature is ~90 K and the bandwidths 20 and 40 MHz, providing resolutions of 0.8 and 3.2 km s^{-1}, respectively, at the rest frequency of 22.235080 GHz. Each source was observed in the total power mode for 3 h; the antenna beam is 90 arc s and covers only the central part of each galaxy.

In Fig. 1 is a spectrum for NGC3079 showing a strong central water vapour feature of ~5 Jy in size and having a width of ~10 km s^{-1}; in addition, there are weaker emission features of <1 Jy extending out to velocities of ±80 km s^{-1} from the central feature. The strongest feature in NGC3079 is blueshifted by ~200 km s^{-1} from the systemic velocity of the galaxy of 1,171 km s^{-1} (ref. 6). In Fig. 2 is a spectrum (taken on the NRAO 300-ft telescope in May 1984) of the absorption by the OH radical at 1667.358 MHz in the radio continuum of NGC3079 (see also B. Turner, I. Kazes and L. J. Rickard, personal communication). This spectrum shows a deep absorption feature ($N_{OH}/T_{EX} = 7.6 \times 10^{15}$ cm^{-2} K^{-1}) at lower velocities than the systemic velocity of the galaxy. The velocity of the H_2O maser emission is indicated lying on the blueshifted edge of the OH absorption, implying that the H_2O maser source is foreground